Supplemental material

Cannon et al., https://doi.org/10.1083/jcb.201807211

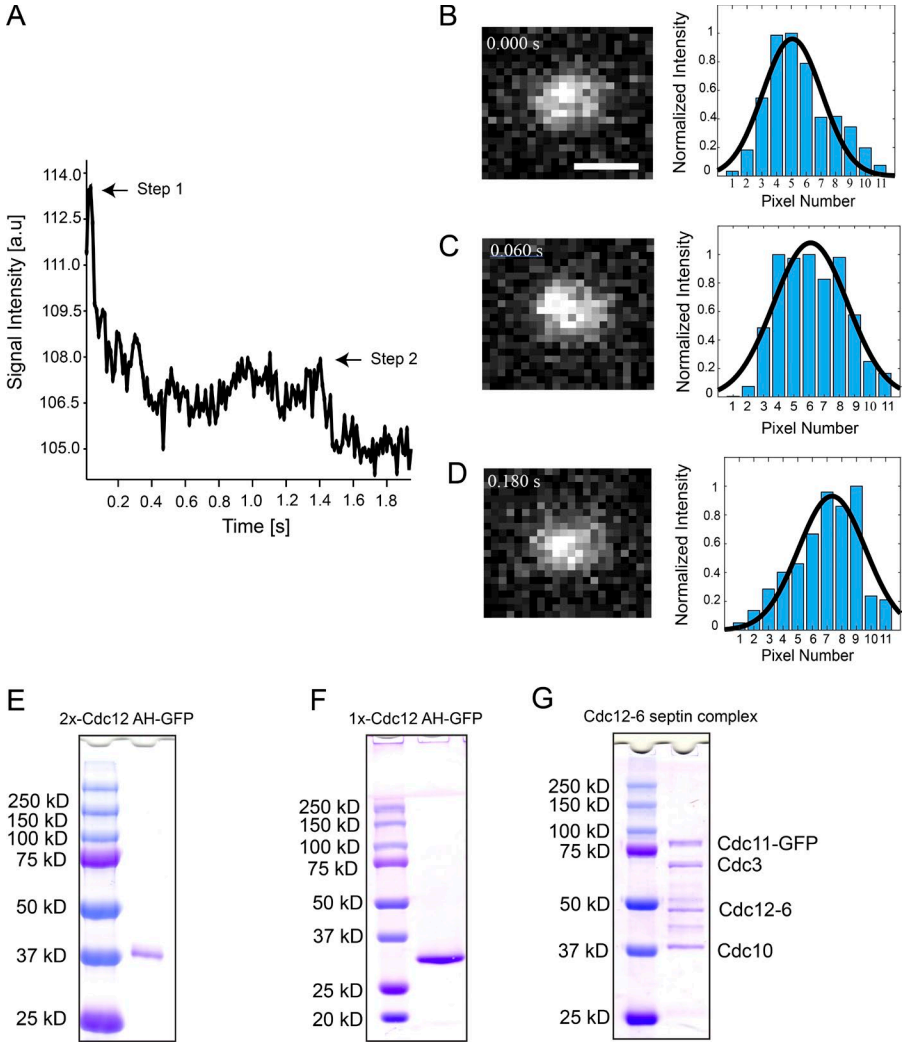

Figure S1. **Single-molecule photobleaching profiles and protein purification. (A)** Two-step photobleaching profile for a single septin complex. **(B–D)** Time lapse imaging of single septin molecules binding to a 1-µm bead (B). A single-septin complex is bound to the bead. Bar, 1 µm. **(C)** A second septin complex binds to the bead, adjacent to the initially bound septin particle. **(D)** A single-septin particle disassociates from the bead. Signal intensity profiles for B–D were all fit to Gaussian distributions. **(E–G)** Coomassie staining of recombinantly expressed 2× Cdc12-AH-GFP, 1× Cdc12 AH-GFP, and yeast septins Cdc11-GFP, Cdc3, Cdc12-6, and Cdc10, after cleavage of 6×-histidine tag via Tobacco etch virus protease, respectively.

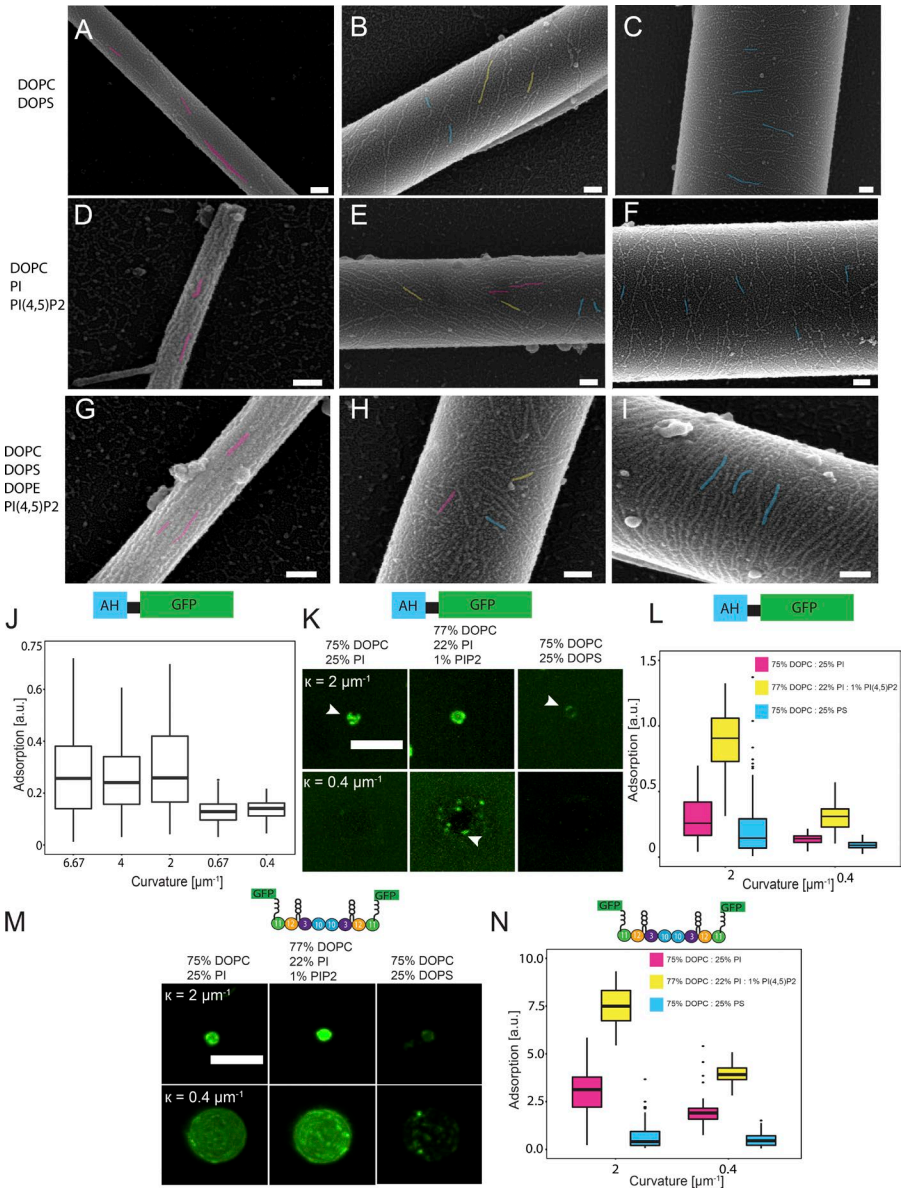

Figure S2. **The effects of lipid composition on septin filament orientation and binding of 1× AH domain and septin complexes onto curved membranes.** SLBs of various lipid compositions were generated onto borosilicate rods. 50 nM purified septins were added to SLBs, and images were acquired using a scanning electron microscope. Representative images were selected from three different categories (100–400 nm, 401–600 nm, and 601–2,300 nm. A subset of filaments were false colored; pink filaments are more parallel to the long axis of curvature; yellow filaments are oriented at ∼45°; blue filaments are aligned to the axis of principal curvature. **(A–C)** Representative images of septin filament alignment on DOPC (75%)- and DOPS (25%)-coated rods. Rod diameters are 195 nm, 470 nm, and 1,096 nm (left to right). **(D–F)** Representative images of septin filament alignment on DOPC (75%)-, PI (20%)-, and $PI_{(4,5)}P_2$ (5%)-coated rods. Rod diameters are 95 nm, 494 nm, and 1,006 nm (left to right). **(G–I)** Representative images of septin filament alignment on DOPC (70%)-, DOPS (10%)-, DOPE (10%)-, and $PI_{(4,5)}P_2$ (10%)-coated rods. Rod diameters are 189 nm, 519 nm, and 1803 nm, respectively. Bars, 100 nm. **(J)** Box and whisker plot quantifying adsorption of 1 μM 1× AH-GFP onto various membrane curvatures with a lipid composition of 75% DOPC, 25% PI, and trace Rh-PE. $n > 74$ beads per curvature. Black bars represent the median, and error bars represent the standard deviation. **(K)** Binding of 1 μM 1× AH-GFP (green) to either κ =2 μm^{-1} or 0.4 μm^{-1} membrane curvatures with various lipid compositions. All images are contrasted identically. White arrowheads highlight filament-like structures. Bar, 5 μm. **(L)** Box and whisker plot quantifying adsorption of 1× AH-GFP onto membrane curvatures with various lipid compositions from K. $n >$ 74 beads per condition. Black bars represent the median, and error bars represent the standard deviation. **(M)** Adsorption of 15 nM septin complex (green) to either κ =2 μm^{-1} or 0.4 μm^{-1} membrane curvatures with various lipid compositions. All images are contrasted identically. Bar, 5 μm. **(N)** Box and whisker plot quantifying adsorption of septin complexes onto membrane curvatures with various lipid compositions from M. $n > 36$ beads per condition. Black bars represent the median and error bars represent the standard deviation.

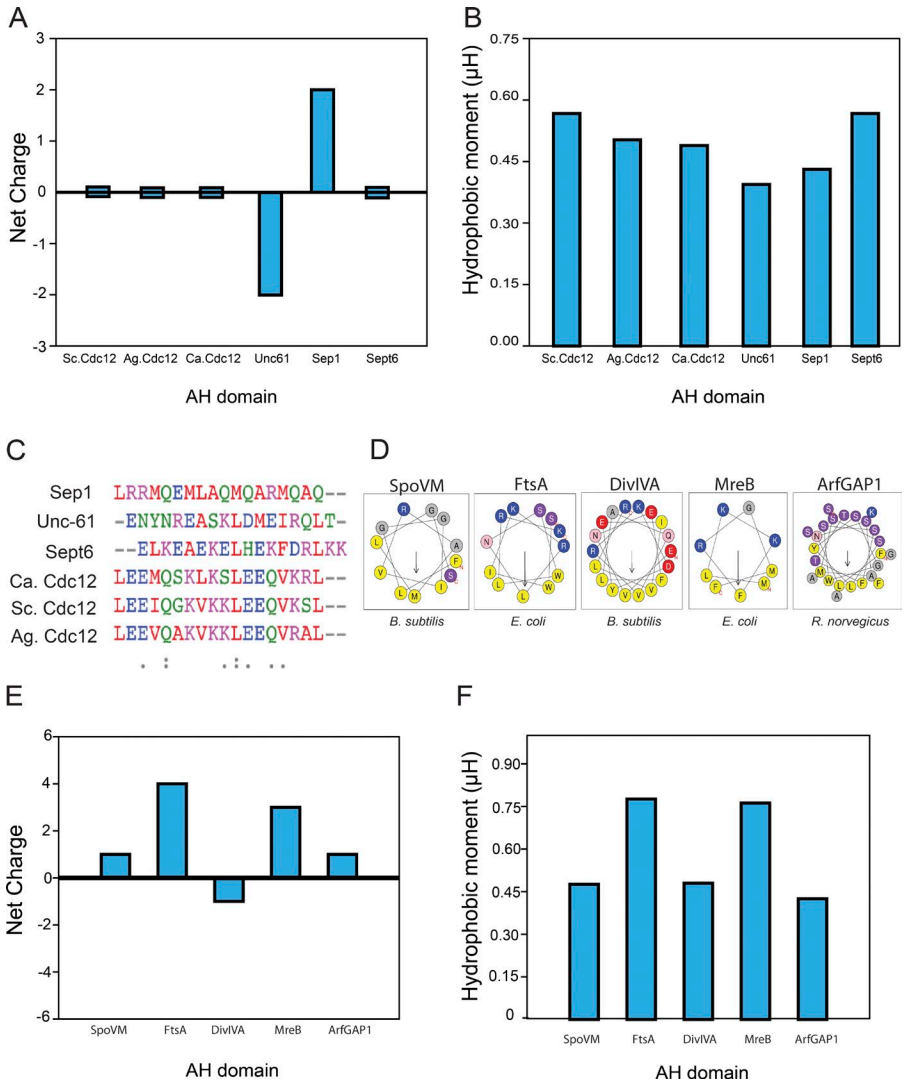

Figure S3. **Septin AHs net charge and hydrophobicity. (A and B)** Net charge and hydrophobic moment of selected septin AHs, respectively. **(C)** Primary sequence alignment of septin AHs. **(D)** Helical wheel diagrams for selected membrane binding and/or curvature-sensing AHs. **(E and F)** Net charge and hydrophobic moment of selected AHs. Interestingly, AH domains with a net charge of zero (*S. cerevisiae*, *Candida albicans*, *A. gossypii*, and *Homo sapiens*) have higher hydrophobic moments than AH domains that are charged (*C. elegans* and *Drosophila melanogaster*). The properties of the AH domain might be tuned to reflect differences in lipid compositions across species, yet still localize to similar membrane geometries. The septin AH hydrophobic moments closely match SpoVM and DivIVA, other micrometer-scale sensors from bacteria.

Tables S1 and S2 are included as separate Microsoft Excel documents. Table S1 shows the biochemical parameters for septin adsorption onto various membrane curvatures. Table S2 shows the coefficient of variation for septin filament alignment on rods.